MAX-PLANCK-GESELLSCHAFT

Journal of Molecular Catalysis A: Chemical, 185 (2002) 1-2, 291-303

Molybdenum oxide based partial oxidation catalyst: Part 3. Structural changes of a MoVW mixed oxide catalyst during activation and relation to catalytic performance in acrolein oxidation

O. Ovsitser[1], Y. Uchida[1], G. Mestl[1]*, G. Weinberg[1], A. Blume[1], J. Jäger[1], M. Dieterle[1], H. Hibst[2] and R. Schlögl[1]

[1]Department of Inorganic Chemistry, Fritz-Haber-Institute of the MPG, Faradayweg 4-6, 14195 Berlin, Germany
[2]BASF AG, ZAK/F-M301, 6056 Ludwigshafen, Germany

* Corresponding author: e-mail mestl@fhi-berlin.mpg.de

Received 09 January 2002; accepted 14 March 2002

Abstract

The activation of a $Mo_9V_3W_{1.2}O_x$ catalyst was investigated in the partial oxidation of acrolein as function of reaction temperature and atmosphere. The activity and selectivity to acrylic acid considerably increased during activation in the acrolein oxidation reaction comparable to the recently reported activation after thermal pretreatment in inert gas. The activation during the catalytic acrolein oxidation, however, proceeds at about 200 K lower temperatures as compared to the inert gas pretreatment. The initial nanocrystalline catalyst structure changed during operation in the acrolein oxidation, as shown by X-ray diffraction (XRD), scanning electron microscopy (SEM), transition electron microscopy and energy dispersive X-ray (EDX) analysis. A $(MoVW)_5O_{14}$-type mixed oxide was found to be the main crystalline phase in the active and selective catalysts. Hence, this $(MoVW)_5O_{14}$ phase crystallizes already during catalysis at the low acrolein oxidation reaction temperatures. The evolution of the catalytic performance is directly related to this low temperature formation of the $(MoVW)_5O_{14}$ phase. It is suggested that this $(MoVW)_5O_{14}$ phase has to be present in a detected, specific ordering state which is vital for optimum selective oxidation properties. In addition, other minority phases were identified by transmission electron microscopy (TEM) in the operating catalyst. The so-called bundle-type, and a new corona-type texture was detected, which show ordering in only one or two dimensions, respectively. These disordered structures are also relevant candidates for active catalyst phases as they are detected during the activation period of the MoVW mixed oxide.

Keywords: Molybdenum; Vanadium; Tungsten mixed oxide catalyst; Acrolein selective oxidation; Mo5O14-type structure; Structure–activity relation; Activation

1. Introduction

MoVW mixed oxide catalysts are industrially used for the oxidation of acrolein to acrylic acid. It is one of the most selective and active oxide catalyst systems. Its selectivity to acrylic acid exceeds 90% at an acrolein conversion above 90%. Moreover, MoVW oxide catalysts are stable at the optimum reaction conditions and operate for years in industry without the need for regeneration. It is not fully clear, however, which phase is present under reaction conditions, and which function has to be attributed to the three main cationic species of the catalyst. Many patents [1, 2, 3, 4 and 5] and several publications deal with MoVWMe oxide catalysts for acrolein oxidation [6, 7, 8 and 9]. Limited and often contradictory data are available in the open literature concerning the structure of the component active for the acrolein oxidation in the mixed MoVMe oxide catalysts. Thus, Mo_3VO_{11+x} was suggested to be an active phase in MoV oxide catalysts [10, 11 and 12]. This phase was proposed to have a β-Mo_4O_{11}-type structure (monoclinic modification) and was formed at 673 K during activation in the acrolein oxidation. On the other hand, an amorphous component of the MoVWMn oxide catalysts was suggested to be active in the acrolein oxidation [8 and 9]. The relative acrolein oxidation activity was found to be proportional to the fraction of the catalyst, which remained uncrystallized. However, cata-

lyst crystallization was conducted in these experiments under air–nitrogen–water atmospheres and at 683 K. Under these conditions, other phases, not being active and selective in acrolein oxidation, can be formed in the mixed oxide catalyst, which would also explain the catalyst deactivation. Again, it was concluded that only X-ray amorphous MoV mixed oxides contained selective oxidation centers in contrast to crystalline samples [13]. In this investigation, catalyst crystallization was also performed in oxidizing atmosphere at 723 K. Hexagonal MoO_3 was detected after such a treatment. Indeed, it cannot be ruled out a priori that the hexagonal MoO_3 structure may exhibit some activity and selectivity for partial oxidation reactions. However, this result does not imply, of course, that other crystalline MoVW mixed oxides are not active and selective in the partial oxidation of acrolein.

In a series of papers, devoted to the study of molybdenum oxide based partial oxidation catalysts, detailed structural studies of MoVWO catalysts were performed to develop a deeper understanding of the relation between catalyst structure and catalytic performance [14, 15 and 16]. In this present work, the activation of a $Mo_9V_3W_{1.2}O_x$ catalyst was studied in the reaction of acrolein oxidation to acrylic acid and is compared to the previously reported activation in inert gas [15, 16 and 17]. Changes of the catalytic performance are compared to changes of the catalyst structure as investigated by X-ray diffraction (XRD), scanning electron microscopy (SEM), transition electron microscopy and energy dispersive X-ray (EDX) analysis. Hence, this study was aimed at the correlation of the development of the catalytic properties of MoVW mixed oxides with their structural evolution during the catalytic acrolein oxidation. Such a structure–reactivity correlation generates additional, more profound information about the active and selective phases in MoVW mixed oxide catalysts for acrolein oxidation.

2. Experimental

The $Mo_9V_3W_{1.2}O_x$ catalyst was prepared from ammonium heptamolybdate, ammonium metatungstate, and ammonium metavanadate as described in [16]. The solution was dried by evaporation and decomposed under nitrogen at 673 K. The obtained mixed oxide will be referred to as the starting material. The catalyst has a BET surface area of 4 m^2/g, which did not change upon the catalyst treatments applied. The sieve fraction of 0.4–0.6 mm from crushed pellets was used for the catalytic measurements.

The experiments were performed in a quartz tubular flow reactor (i.d. 4 mm). The catalyst (0.025–0.1 g) was diluted with quartz (1:10–1:4 w/w) to achieve a better temperature control. Reaction mixtures of 4–8% C_3H_4O, 6–20% O_2, 20% H_2O, and the balance He with total flow rates of 0.2–2 ml/s were used for the catalytic measurements. The reactants and products were analyzed with an on-line gas chromatograph (Varian 3800) equipped with TCD and FID detectors. A Porapak-QS column (2 m×1/8 in., ss) and a 60/80 Carboxen™ 1000 column (15 FTs×1/8 in., ss) were employed for the analysis of permanent gases and organic substrates. The carbon mass balance was 100±5%.

XRD measurements were done at room temperature on a STOE STADI-P focusing monochromatic transmission diffractometer equipped with a with Ge(1 1 1) monochromator and a position-sensitive detector. Cu Kα radiation was used. The phase analysis was performed with the STOE Win XPOW (version 1.06; Stoe Darmstadt, Germany) software package and with PowderCell (V 2.3; Bundesanstalt für Materialforschung und -prüfung (BAM) Berlin, Germany).

SEM was conducted with the Hitachi S-4000 microscope (Hitachi). The acceleration voltages were set at 15 and 25 kV and the working distances at 8 and 18 mm to probe different sample thickness. Transmission electron microscopy (TEM) images and selected area electron diffraction (SAED) were recorded on the CM 200 FEG microscope (Philips). The acceleration voltage was set at 200 kV. Energy dispersive analyzers (EDX) (DX 4, EDAX Inc.) equipped with Li-doped Si crystals are attached to both SEM and TEM microscopes for element analysis. In total, a number of nine and eight different EDX analyses were performed for each sample at different spots. The EDX data were automatically corrected for sample absorption by the EDX software package.

3. Results

3.1. Catalytic performance and XRD analysis

Fig. 1 shows the conversion of over the $Mo_9V_3W_{1.2}O_x$ catalyst in the acrolein oxidation at 533–573 K and at τ =0.04 g s/ml as a function of time on stream. The catalytic activity of the starting material increased considerably during operation in the reaction. The initial activity was close to

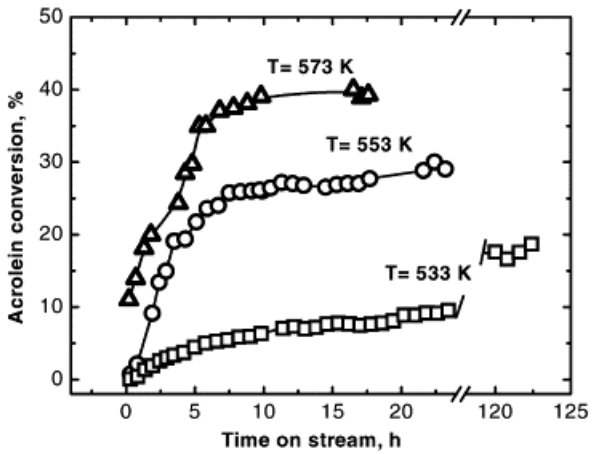

Fig. 1. Acrolein conversion over the $Mo_9V_3W_{1.2}O_x$ catalyst at 533 K (open squares), 553 K (open circles), and 573 K (open, bold triangles) and τ=0.04 g s/ml as a function of operation time on stream. Reaction mixture composition: 4% C_3H_4O, 10% O_2, 20% H_2O, balance He.

0, which indicates the majority of active sites being formed only during the activation procedure. The activation time required was related to the reaction temperature. At activation temperatures between 553 and 573 K, the catalyst activity increases sharply during the first 5–10 h of operation in

the reaction. Subsequently, the activity increases only slightly during the next 20–40 h. For the activation temperature of 533 K, a slight increase in the catalyst activity was still observed even after 120 h of operation (Fig. 1). This long-time period of activation points to structural alterations within the mixed oxide catalyst. XRD, SEM, TEM and EDX analyses were applied to identify these structural changes in the catalyst during the activation period.

As reported in [14, 15 and 16], a nanocrystalline Mo_5O_{14}-type mixed oxide was observed as the major phase by XRD after preparation and calcination at 673 K with a minor amount of nanocrystalline MoO_3-type oxides. The XRD pattern of the catalyst activated in the reaction of acrolein oxidation after reaching the steady-state level is displayed in Fig. 2 (pattern 2) together with the XRD pattern of the initial material (pattern 1). A theoretical pattern (Fig. 2, pattern 3)

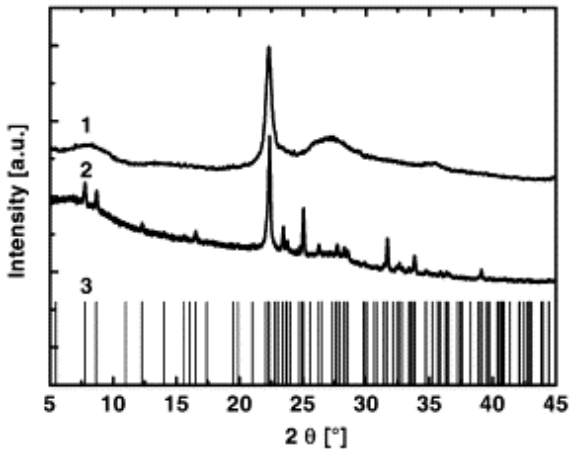

Fig. 2. XRD pattern of the initial material (1), $Mo_9V_3W_{1.2}O_x$ catalyst activated in the reaction (2) and powder reference data (3) as calculated for the tetragonal space group P4/mbm (127).

was calculated as reference. Based on the single crystal structure analysis of the binary oxide Mo_5O_{14}, the tetragonal space group P4/mbm (127) was used to calculate the possible hkl-values for the given structure with the lattice parameter a=2277.2 pm and c=397.9 pm. Unfortunately, single crystal XRD data are only available in the literature for the binary Mo_5O_{14}, and not yet for the ternary and quaternary mixed oxides. Therefore, all intensities were set to 30% relative to the experimental data because information about site occupation or site distribution of the three different transition metal atoms in the structure are not available. Hence, correct intensities cannot be simulated. Even XRD powder reference data for mixed oxides of the Me_5O_{14}-type structure is limited to only $(Mo_{0.93}V_{0.07})_5O_{14}$. A good correspondence in position was observed between the experimental pattern and the reference data indicating that the Mo_5O_{14}-type mixed oxide is the major crystalline phase in the $Mo_9V_3W_{1.2}O_x$ catalyst after activation in the reaction. The crystallization to the $(MoVW)_5O_{14}$-type mixed oxide, thus, could be one explanation for the increasing activity and selectivity in the acrolein oxidation.

To prove this hypothesis, $Mo_9V_3W_{1.2}O_x$ samples with different fractions of the crystalline Mo_5O_{14}-type phase were tested in the acrolein oxidation under identical reaction conditions (T=533 K, reaction mixture composition: 4% C_3H_4O, 8% O_2, 20% H_2O, τ=0.03 g s/ml). As reported in the previous paper [16], thermal treatment of the initial material in inert gas also resulted in the crystallization of the Mo_5O_{14}-type phase, however, at significantly higher temperatures (803–818 K). Thermal treatment at temperatures above 829 K led to the decomposition of the metastable Mo_5O_{14}-type phase to stable MoO_3 and MoO_2 [16]. Results on the rate of acrolein oxidation with time on stream over such differently activated catalysts are summarized in Fig. 3. As seen, maximum activity was reached for the sample activated in inert gas at 813 K (trace 4 of Fig. 3). This catalyst contained a maximum amount of the Mo_5O_{14}-type phase [16]. The selectivity to acrylic acid exceeded 90% at applied conditions for all tested samples, except the first data points measured for the initial, not activated material (trace 1 of Fig. 3.). For all thermally activated catalysts, a high level of activity was observed already for the first hours of operation in the reaction (Fig. 3).

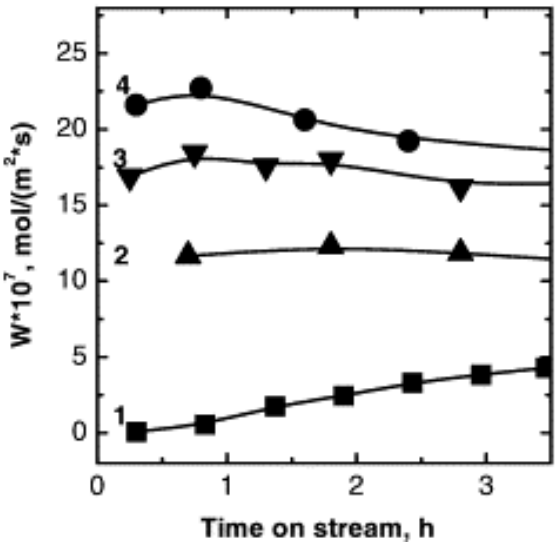

Fig. 3. Rate of acrolein oxidation over the $Mo_9V_3W_{1.2}O_x$ catalyst at 533 K thermally treated in inert gas: (1) initial, not activated material (filled squares), (2) thermally treated at 829 K (filled, upward triangles), (3) thermally treated at 803 K (filled, downward triangles) and (4) thermally treated at 813 K (filled circles). Reaction mixture composition: 4% C_3H_4O, 10% O_2, 20% H_2O, balance He.

The acrolein conversions at 543 K and τ=0.03 g s/ml are displayed in Fig. 4A which were measured for the initial, not activated material (1) and over the $Mo_9V_3W_{1.2}O_x$ catalyst thermally activated in inert gas at 813 K (2). The selectivities of both samples are displayed in Fig. 4B. The initial $Mo_9V_3W_{1.2}O_x$ catalyst eventually reached the same levels of activity and selectivity in the process of activation in the reaction mixture as the catalyst thermally activated in inert gas at 813 K, which showed this high performance from the first hours of operation in the reaction.

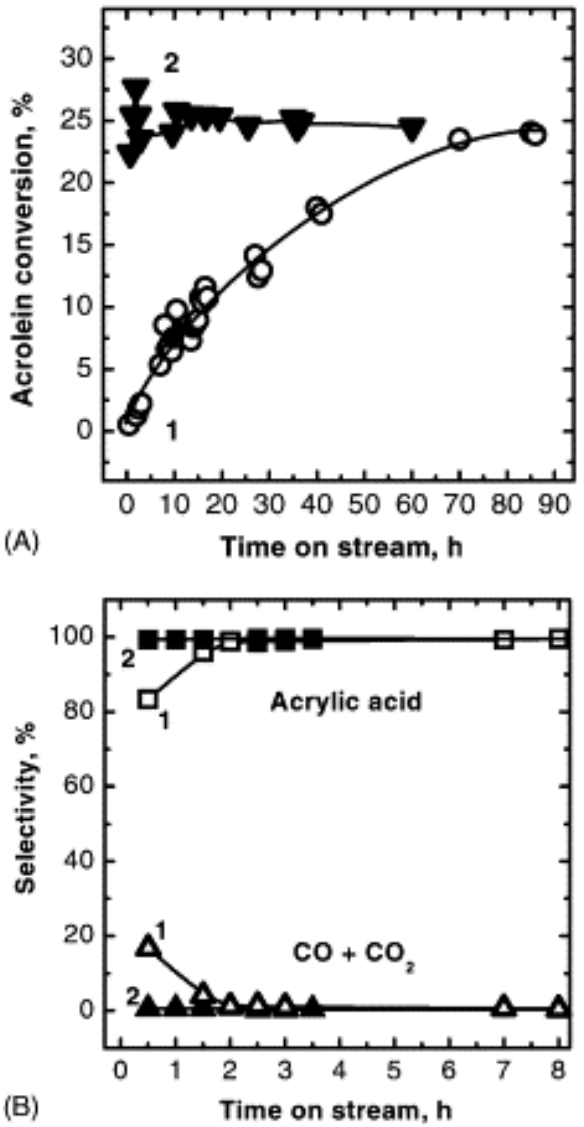

Fig. 4. Acrolein conversion (A) and selectivities (B) at 543 K and τ=0.03 g s/ml over (1) the initial material (open symbols), and (2) over the $Mo_9V_3W_{1.2}O_x$ catalyst thermally activated in inert gas at 813 K (filled symbols).

The XRD patterns of the $Mo_9V_3W_{1.2}O_x$ catalysts thermally activated in inert gas at 818 K and activated in the reaction are compared in Fig. 5. It is evident that the Mo_5O_{14}-type oxide crystallized in both samples during the treatments in the reaction or in inert gas. The catalyst activated in inert gas also contained an additional phase, which is indicated in Fig. 5 by the + signs. The XRD pattern of this additional phase is similar to that of $(MoV)_2O_{5-x}$ as described by Uchida et al. in detail [18]. The lattice parameter *a* of the Mo_5O_{14}-type oxide increased by 10 pm after the reaction to *a*=2287 pm, while the *c*-axis remained unchanged with 398 pm. The reason for this expansion in *a* direction may be due to disorder such as an inhomogeneous loss of metal atoms from the Mo_5O_{14}-type oxide. It was reported that catalytic action led to considerable changes in the metal distribution in the Mo-V-W mixed oxide catalyst as shown by XPS analysis as well as SEM–EDX, and TEM–EDX mapping [15]. Such a V loss, hence, might explain the observed lattice expansion. Attempts to simulate such a loss of metal atoms, however, did not lead to correct results. On the other hand, such a V loss could also be related to the XRD observation of a second, minority phase, $(MoV)_2O_{5-x}$.

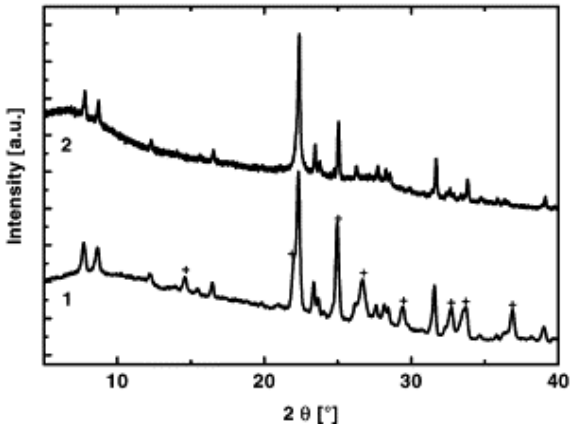

Fig. 5. XRD patterns of the $Mo_9V_3W_{1.2}O_x$ catalyst thermally activated in inert gas at 818 K (1) and activated in the reaction (2). Crosses indicate the additionally identified $(MoV)_2O_{5-x}$.

3.2. SEM and EDX analysis

The SEM analysis of initial material (thermally treated in inert gas at 673 K) did not reveal the presence of crystallized materials as indicated by the irregular particle morphologies (images not shown). SEM–EDX analysis revealed heterogeneous elemental distribution (data not shown). For the initial, not activated material, the Mo content varied from 63 to 67 at.%, the V content from 20 to 27 at.% and the W content from 10 to 13 at.%.

Activation of the catalyst in the reaction of acrolein oxidation at temperatures lower than the temperature of thermal treatment of the initial material results in the formation of well-defined particles of different morphologies (Fig. 6). Needle-like (Fig. 6A), platelet-like (Fig. 6B and C) as well as spherical particles (Fig. 6D) were detected for the catalyst after activation in the reaction mixture. Similar morphologies were observed after thermal activation in inert gas at 803–818 K [15]. SEM–EDX analysis revealed an increase of the heterogeneity in the elemental distribution after activation in the reaction (Fig. 6). For such activated samples, the V content varied from 19 to 29 at.%, the Mo content from 60 to 69 at.%, and the W content from 11 to 13 at.%.

As clearly seen from Fig. 6, the activation in the reaction of acrolein oxidation at temperatures between 533 and 603 K results in the formation of the crystalline phases. These temperatures are lower than the temperature of the thermal treatment of initial material (673 K), for which the presence of crystallized material again was not detected [14, 15, 16 and 17]. This observation clearly indicates an acceleration of the crystallization process under the reaction conditions.

Samples deactivated in the reaction (*T*=673 K, reaction mixture composition: 8% C_3H_4O, 20% O_2, 20% H_2O, rest He) were characterized by still a higher degree of crystallinity as

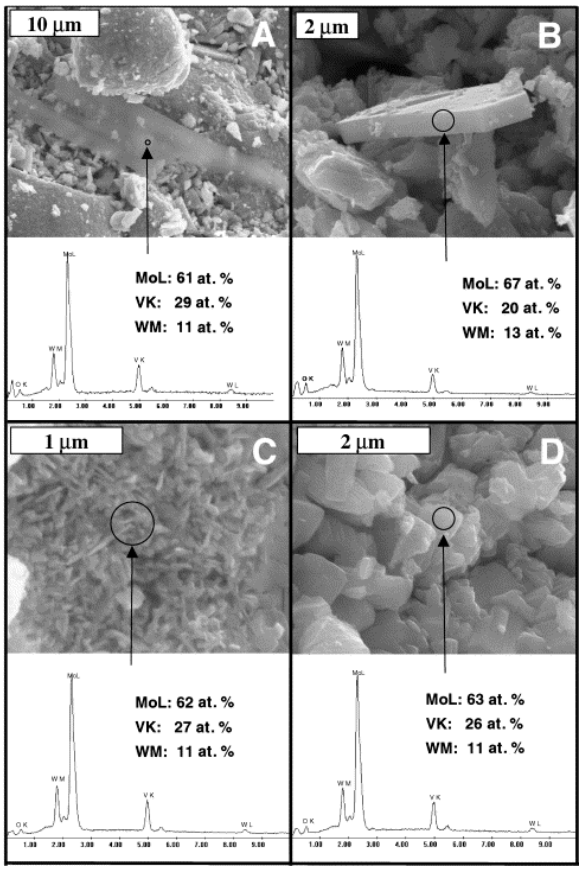

Fig. 6. SEM images and EDX data of the $Mo_9V_3W_{1.2}O_x$ catalyst activated in the acrolein oxidation. Arrows indicate the spots of the EDX analysis.

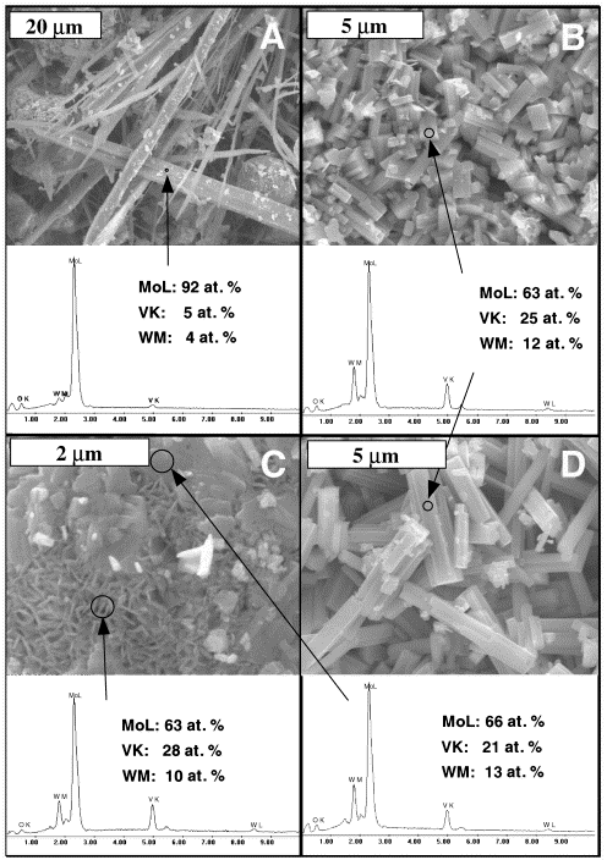

Fig. 7. SEM images and EDX of the $Mo_9V_3W_{1.2}O_x$ catalyst deactivated at 673 K in the acrolein oxidation. Arrows indicate the spots of the EDX analysis.

indicated by SEM (Fig. 7A–D) and a higher heterogeneity in the elemental distribution as shown by EDX (Fig. 7). Thus, the Mo content of such samples varied from 60 to 92 at.%, the V content from 4 to 25 at.%, and the W content from 4 to 14 at.%. This increased elemental heterogeneity indicates the beginning disproportionation of the Mo_5O_{14}-type phase to MoO_2- and MoO_3-type phases as described earlier [16].

3.3. HR-TEM of samples activated in the reaction

As already mentioned above, the initial material has been thermally treated at 673 K prior to catalysis in order to decompose the ammonium salt precursors. High resolution transmission electron microscopy (HR-TEM) did not reveal the presence of well-crystallized particles (images are not shown) in agreement with previous results [14, 15 and 16].

HR-TEM confirmed the formation of the $(MoVW)_5O_{14}$-type structure being well crystallized in the samples activated in the reaction. Fig. 8A displays one HR-TEM image and the SAED pattern obtained from the $(MoVW)_5O_{14}$-type structure, and an optical power spectrum as calculated from the displayed HR-TEM image. The well resolved lattice fringes, and the high similarity of the power pattern with the well resolved SAED pattern confirm the high degree of crystallinity of this particle. It is important to note that this phase was detected in the $Mo_9V_3W_{1.2}O_x$ catalyst, which was activated in the acrolein oxidation reaction. Fig. 8B shows the HR-TEM image, the SAED pattern, and an optical power spectrum as calculated from the HR-TEM image of a MoO_3-type crystal detected in the MoVW mixed oxide activated in the acrolein oxidation reaction. The detected MoO_3-type crystals, however, are thought to have the usual MoO_3-type structure, despite of the observation of symmetry-forbidden diffraction 001 spots in addition to the regular (0 0 2) spots. Forbidden diffraction spots are often observed in the diffraction pattern of oxide crystals irradiated in the electron beam. Therefore, the detection of these spots most probably is caused by the irradiation during the adjustment of the crystal.

In addition, a bundle-like texture was also detected by HR-TEM after activation in the acrolein reaction depending on the temperature and time periods used. Fig. 8C exhibits one respective HR-TEM image (particle size: up to maximum 50 nm in diameter) of this phase, the SAED, and the optical power pattern as calculated from the HR-TEM image. As previously reported [16], this so-called bundle texture is characterized by the only detectable lattice distance of 390 pm and understood as a two-dimensionally ordered structure. However, it is important to note that this so-called bundle texture was detected in the present study from the beginning of the crystallization of the Mo_5O_{14}-type structure, in contrast to the previous work, where this type of texture was only observed for samples in which the Mo_5O_{14}-type structure began to disproportionate to MoO_2- and MoO_3-like oxides. This difference might be explained by the

different activation treatments, the activation in the acrolein oxidation reaction, and in inert gas [16]. Alternatively, it can also not be excluded that both so-called bundle textures belong to two structures differently organized at the local scale, but having the same 390 pm lattice parameter. Unfortunately, this bundle textures is so disordered that diffraction pattern which would yield more information can not be obtained.

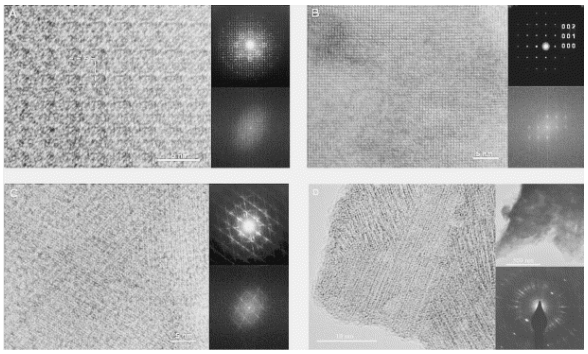

Fig. 8. Electron micrographs, SAED patterns and power spectra of the Mo9V3W1.2O*x* catalyst activated at $T = 533–603$ K: (A) (MoVW)5O14-type structure, (B) unusual MoO3-type structure, (C) bundle-type structure and (D) corona-type structure.

Mo_4O_{15}-type, MoO_3-type, and bundle-like textures were already observed previously in the catalyst thermally treated in inert gas at 813–829 K [16]. However, it must be pointed out that, in the present investigation, these structures have crystallized in catalysts, which were activated in the acrolein oxidation reaction at significantly lower temperatures (533–603 K). Hence, these HR-TEM observations are very important as they prove that the crystallization of such phases is enhanced during catalysis as compared to inert gas treatment.

In addition to the earlier described structures, a new, corona-type texture was observed too after activation in the reaction between 533 and 573 K. Fig 8D shows a respective HR-TEM image of a particle (particle size: up to maximum 50 nm in diameter), an overview image and the SAED pattern of this phase. This corona-type texture was never observed in samples activated in inert gas, which were previously described in detail [16]. It is again characterized by a distance of the lattice fringes of 390 pm. It is understood as a texture being only one-dimensionally ordered. Moreover, the corona-type, like the bundle-like texture, was detected at the very initial stage of the activation in acrolein oxidation, i.e. in the samples activated in the reaction at 533 K only for 3 h. Hence, both disordered structures already form at early stages of the activation/crystallization process. In this sense, both structures might be intermediate stages of the crystallization of $(MoVW)_5O_{14}$, which is indeed characterized by the layer distance of 390 pm. The structural evolution of $(MoVW)_5O_{14}$ then could be imagined as starting from the nanocrystalline precursor, over the corona-type texture, in which only stacking order in one dimension occurs, and the bundle-type texture, in which the layers gradually order, to finally the crystalline $(MoVW)_5O_{14}$-type oxide.

These HR-TEM observations may shed new light on the potential role of such disordered phases for catalysis. Since, these structures are one- (corona-type), and two-dimensionally (bundle-like) ordered, they also could be relevant candidates for active MoVW mixed oxide catalysts phases.

Furthermore, the formation of a new $(Mo_{0.6}V_{0.3}W_{0.1})_2O_{5-x}$ crystal phase was detected in the $Mo_9V_3W_{1.2}O_x$ catalyst after activation in the acrolein oxidation for a more reducing reaction mixture composition (4–5% C_3H_4O, 7–8% O_2, 20% H_2O, balance He). The identification and discussion of this phase, however, is beyond the scope of this catalysis paper and will be discussed in detail in a publication devoted to TEM [18].

Finally, catalyst deactivation at T=673 K (reaction mixture composition: 8% C_3H_4O, 20% O_2, 20% H_2O, rest He) resulted in the already well described formation of typical MoO_3-type crystals (images not shown) as evidenced by HR-TEM in accordance to previous work [15, 16 and 17].

The dark field (DF) imaging TEM technique was applied to identify the formation of nanocrystalline phases in the surface-near layers of the $Mo_9V_3W_{1.2}O_x$ catalyst activated in the reaction. The DF electron micrograph in Fig. 9B has been obtained with the diffracted electron beam as schematically shown in the diffraction pattern in the Fig. 9. The indicated small ring on the 390 pm diffraction ring in this diffraction pattern shows the position and diameter of the objective aperture, which has been inserted at the focal plane of the objective lens of the electron microscope. The imaging procedure has been performed with a tilted incident electron illumination, thus, the diffracted electron beam remained on the optical axis of the objective lens. Under this imaging condition, only those crystals are observed as bright features in the DF image, for which the diffracted electron beams can pass through the inserted objective aperture, i.e. which fulfill the Bragg condition. Other crystals, which satisfy the diffraction condition for incident electron wave but do not for the diffracted electron beams, i.e. the diffracted beam does not pass through the objective aperture, cannot create a bright contrast in the imaging focal plane. Amorphous components and other crystalline phases in the sample, which do not satisfy this diffraction condition, thus, do not contribute to the bright contrast. Because of the extremely small nanocrystallites, the electron beam was directed under diffraction conditions at one set of bright spots seen in the 390 pm diffraction ring of the SAED pattern shown in right of Fig. 9. Under these diffraction conditions, all nanocrystallites will appear as bright features in the DF image. Positioning the objective aperture at another group of spots in this ring will result in the appearance of nanocrystallites at other locations in the DF image (not shown).

The bright field (BF, Fig. 9A) and DF (Fig. 9B) images are compared on the left and in the center of Fig. 9. This comparison of the BF and DF images identifies the formation of small nanocrystallites in the surface-near layers of

$Mo_9V_3W_{1.2}O_x$ catalyst particles activated in the acrolein oxidation reaction. From the obtained results, however, a

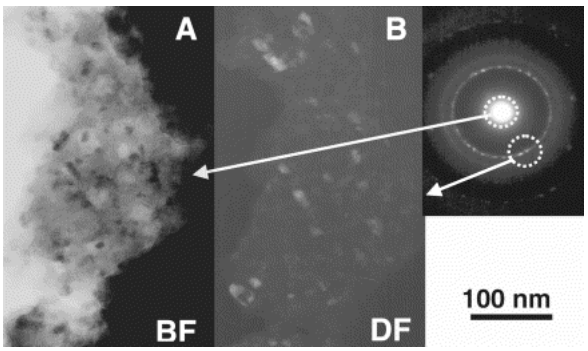

Fig. 9. Electron micrographs (left and center) and SAED pattern (right) of the nanocrystallites formed in the surface layer of the $Mo_9V_3W_{1.2}O_x$ catalyst activated in the reaction: (A) BF imaging and (B) DF imaging.

definite conclusion about the geometric structure of these nanocrystallites cannot be drawn, except the 390 pm lattice distance. It should be noted that this lattice distance is in accordance with the one calculated from the prominent XRD diffraction line of the nanocrystalline starting material (Fig. 5, pattern 1). HR-TEM thus supports the XRD finding.

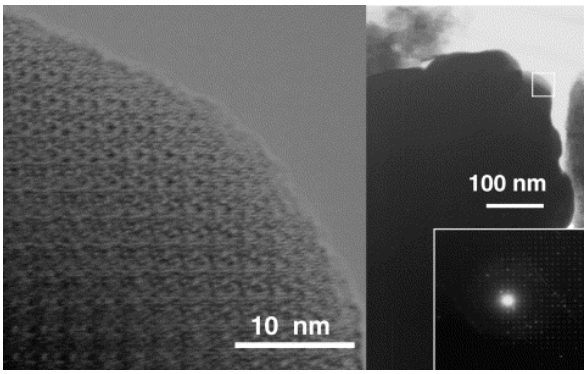

Fig. 10. HR-TEM image (left), TEM image (top right), and SAED pattern (bottom right) of the $(MoVW)_5O_{14}$-type crystal, formed on the surface layer of the $Mo_9V_3W_{1.2}O_x$ catalyst activated in the acrolein reaction. The square in the TEM image (top right) indicates the area of the HR-TEM analysis (left).

Additionally, relatively large (50 nm) crystals of the $(MoVW)_5O_{14}$-type structure were already formed after this treatment in the surface-near regions of $Mo_9V_3W_{1.2}O_x$ catalyst particles as also proven by HR-TEM (Fig. 10). Moreover, the HR-TEM image of Fig. 10 reveals, in addition to the resolved lattice fringes of the bulk Mo_5O_{14} structure, that a surface layer of about 2–4 nm thickness of this crystal does not exhibit the regular Mo_5O_{14}-type structure. This observation can only be partly attributed to thickness variations at the outermost surface layer of a few hundred picometer. It seems to be a general observation for such type of oxides that the surface does not terminate in the bulk structure. However, at present it also cannot be excluded that such surface layers are due to electron beam damage in the microscope.

In summary, TEM revealed that the majority of the crystallites, which were formed in $Mo_9V_3W_{1.2}O_x$ catalyst during activation in the reaction, were localized at the particle surfaces. Hence, it can be concluded from the combined HR-TEM results that crystallization of $(MoVW)_5O_{14}$ starts at nanocrystallites located in surface-near regions of mixed oxide particles, and might proceed via the suggested route from the nanocrystalline precursor via corona-like, and bundle-type phases.

4. Discussion

The activity of the initial nanocrystalline material (Fig. 1) is close to zero. Therefore, the initial material constituting the $Mo_9V_3W_{1.2}O_x$ catalyst can be excluded to be an active phase for acrolein oxidation. The significant increase in the catalyst activity (Fig. 1) indicates that the majority of the active sites for acrolein oxidation are formed during the activation in the reaction. It has to be noted that the observed long activation periods at temperatures close to the optimum acrolein reaction temperature indicate that the increase in activity is not related to surface desorption processes, e.g. desorption of water or ammonia, or surface reduction processes, which occur on a much faster time scale, but may be related to the observed formation of an active crystalline phase.

The activation in the reaction of acrolein oxidation at temperatures between 533 and 603 K indeed induces crystallization as confirmed by XRD analysis and electron microscopy investigations (SEM, TEM). These phase transformations take place at temperatures between 523 and 603 K, which are 70–150 K lower than the temperature of the initial thermal treatment of the catalyst (673 K) and 200–300 K lower, than temperatures of crystallization of the $(MoVW)_5O_{14}$-type phase in inert gas (803–818 K) [16]. This indicates an acceleration of the Mo_5O_{14} phase formation under acrolein reaction conditions, probably due to surface reduction and formation of oxygen vacancies. Thermal activation in inert gas at 803–818 K [16], and the activation in the reaction of acrolein oxidation at 533–603 K results in the formation of similar phases (Fig. 5). The $(MoVW)_5O_{14}$-type phase was the main crystalline phase found in both cases, in the samples activated in the reaction, as well as in the samples thermally treated in inert gas at 813–818 K [16].

The initial rates of the acrolein conversion at 533 K over samples thermally activated at 833–829 K (Fig. 3) correlate well with the fraction of the crystalline $(MoVW)_5O_{14}$-type phase in the catalyst material. It is interesting that a similar correlation was also observed between the formation of the $(MoVW)_5O_{14}$-type phase and its catalytic performance in the methanol and propene partial oxidation [15, 16 and 17].

However, it must be mentioned that XRD analysis is not well suited to detect defective structures in particular at the particle periphery. A correlation between volume-sensitive XRD measurements and surface-sensitive reaction rates can

only be observed, when crystalline phases are formed or decomposed more or less homogeneously throughout the whole catalyst volume. Exactly, this case was observed during the thermal treatment of the catalyst in inert gas at high temperatures (803–829 K) [16]. During activation in the reaction at lower temperatures (523–603 K), the catalyst surface, however, may be reduced prior to the bulk, which may accelerate the crystallization and formation of suboxides in the surface-near layers. Due to the low acrolein oxidation reaction temperatures in the present study, the crystallization of the $(MoVW)_5O_{14}$-type oxide proceeds to the volume significantly slower than during the thermal activation in inert gas and at high temperatures [16]. However, small $(MoVW)_5O_{14}$-type crystallites at the particle surfaces, which escape XRD detection, may be sufficient for the catalytic reaction. The crystallization process of $(MoVW)_5O_{14}$ slowly continues with operation time on stream and eventually extends to the catalyst volume. In this case of a core–shell-type phase transition, a full correlation between the fraction of the crystalline phase and the catalytic performance cannot be expected anymore.

TEM confirmed the formation of relatively large (50 nm) crystals of the $(MoVW)_5O_{14}$-type structure (Fig. 10) in the surface-near regions of $Mo_9V_3W_{1.2}O_x$ catalyst particles activated in the reaction. TEM also revealed that majority of the nanocrystallites, which were formed in the $Mo_9V_3W_{1.2}O_x$ catalyst during activation in the reaction, indeed were also localized in the surface-near zones of the particles (Fig. 9). These TEM observations prove the suggested core–shell nucleation-growth mechanism of crystallization starting at the surface (nucleation) and extending to the bulk (growth) at later stages. It is suggested that the catalytic activity develops with the crystallization (nucleation) of these nanocrystallites at the particle surfaces.

In case of the thermally activated catalysts, a high level of activity was observed from the first hour of operation in the reaction (Fig. 3). These results support that the $(MoVW)_5O_{14}$-type oxide could be the active phase for acrolein formation. A long activation period was not required when this phase was preformed.

Due to the variable valence of Mo and V, different phases can be formed in the V-Mo-Me-O system, depending on the chemical composition, reaction temperature and reducing potential of the reaction media. The $(MoVW)_5O_{14}$-type phase is thermodynamically less stable than Mo_4O_{11}, MoO_3, and MoO_2, and more likely represents the active phase in catalysts, which are effective for acrolein oxidation at low temperatures.

The $(MoV)_4O_{11}$-type phase, described by Andruchkevich et al. [10, 11 and 12], as well as other suboxides, also can perform in the acrolein oxidation. However, in our opinion, the $(MoVW)_5O_{14}$-type phase is able to catalyze the acrolein oxidation with a high activity and selectivity to acrylic acid due to its optimum structure, optimum bonds lengths and optimum arrangement of V, W and Mo, and high oxygen mobility. The acrolein conversion rates of 10×10^{-7} to 20×10^{-7} mol/(m^2 s) observed over the $Mo_9V_3W_{1.2}O_x$ catalyst at 533 K (Fig. 3) are approximately 10–100 times higher than the corresponding reaction rates reported for the Mo-V-O catalysts with a Mo_4O_{11}-type structure [12]. Certainly, such an extrapolation is quite approximate and it would be interesting to measure the reaction rates of different MoVW structures under identical reaction conditions.

In this context, the two disordered phases, the bundle-like, and the corona-type textures, being two- and one-dimensionally ordered have to be discussed as relevant candidates for active catalysts phases. Unfortunately, their inherent structural disorder does not allow further statements about their detailed geometric structure at present.

The TEM observation of structurally ill-defined surface layers on top of crystalline cores of the $(MoVW)_5O_{14}$-type oxide being activated in the selective oxidation of acrolein, however, could be highly relevant for the understanding of the catalytic process. This observation is in full agreement with those reported recently on a thermally activated MoVW catalyst [15 and 16]. A core–shell model was proposed from the combined results [15], in which the crystalline $(MoVW)_5O_{14}$-type core is essential for catalysis due to its electron and oxygen storage capacity. The structurally ill-defined surface layer, on the other hand, may provide the catalytically active and selective centers.

There are still many open questions about the optimum crystallite size, and whether it is necessary for the active catalyst to have a regular structure in all three dimensions. Irregularity and small crystallite sizes may favor the catalyst selectivity and activity due to easy oxygen diffusion, and may facilitate the formation of the active phase. However, the identification of the $(MoVW)_5O_{14}$ phase being the majority species in catalysts activated in the acrolein oxidation reaction for the first time allows the tailored synthesis of this phase and its investigation during the catalytic partial oxidation of acrolein by suited physicochemical techniques.

5. Conclusion

The activity of the $Mo_9V_3W_{1.2}O_x$ catalyst and the selectivity to acrylic acid increased considerably during the operation in the acrolein oxidation. These changes in the catalytic performance could be related to the crystallization of the $(MoVW)_5O_{14}$-type oxide at such low temperatures, as confirmed by XRD, electron microscopy (SEM, TEM). The presented experiments point to the important role of the $(MoVW)_5O_{14}$-type structure for acrolein partial oxidation. Hence, the $(MoVW)_5O_{14}$-type structure is considered as a candidate for the active component in multi-element mixed oxide catalysts. This phase crystallizes via corona-type and bundle-type textures, which are one- and two-dimensionally ordered. It is suggested that this $(MoVW)_5O_{14}$-type phase has to be present in the active catalyst in a specific ordering state comprising a crystalline core and an irregular shell, which is vital for the selective oxidation.

Preprint of the Department of Inorganic Chemistry, Fritz-Haber-Institute of the MPG *(for personal use only)* (www.fhi-berlin.mpg.de/ac)

References

1. A. Tenten, F.-G. Martin, H. Hibst H., L. Marosi, V. Kohl, BASF AG, EP 668104 B1 (1995).
2. T. Kawajiri, S. Uchida, H. Hironaka, Nippon Shokubai Kagaku, EP 427 508 A1 (1991).
3. V. Novak, L. Sokol, J. Jelinek, CS 1207807 B (1981).
4. N. Bertolini, S. Ferlazzo, US Patent 4289654 (1981).
5. A.N. Kurtz, R.W. Cunningdam, A.W. Naumann, US Patent 4111983 (1978).
6. S. Breiter, M. Estenfelder, H.-G. Lintz, A. Tenten and H. Hibst *Appl. Catal. A.* **134** (1996), p. 81.
7. K. Krauss, A. Drochner, M. Fehlings, J. Kunert and H. Vogel *J. Mol. Catal. A: Chem.* **162** (2000), p. 413.
8. L.B. Levy and P.B. Groot *J. Catal.* **76** (1982), p. 385.
9. P.B. Groot and L.B. Levy *J. Catal.* **76** (1982), p. 393.
10. T.V. Andrushkevich and T.G. Kuznetsova *Kinet. Katal.* **27** 2 (1986), p. 571.
11. L.M. Plyasova, L.P. Solov'eva, G.N. Kryukova and T.V. Andrushkevich *Kinet. Katal.* **31** 6 (1989), p. 1253.
12. T.V. Andrushkevich *Catal. Rev. Sci. Eng.* **35** 2 (1993), pp. 213–259.
13. H. Vogel, R. Böhling and H. Hibst *Catal. Lett.* **62** (1999), p. 71.
14. H. Werner, O. Timpe, D. Herein, Y. Ushida, N. Pfänder, U. Wild and R. Schlögl *Catal. Lett.* **44** (1997), pp. 153–163.
15. G. Mestl, Ch. Linsmeier, R. Gottschall, M. Dieterle, J. Find, D. Herein, J. Jäger, Y. Uchida and R. Schlögl *J. Mol. Catal. A: Chem.* **162** (2000), pp. 455–484.
16. M. Dieterle, G. Mestl, J. Jäger, Y. Uchida and R. Schlögl *J. Mol. Catal. A* **174** (2001), pp. 169–185.
17. M. Dieterle, Ph.D. Thesis, TU Berlin, 2001-06-11.
18. Y. Uchida, G. Mestl, O. Ovsitser, R. Schlögl, A. Blume, manuscript in preparation.

Preprint of the Department of Inorganic Chemistry, Fritz-Haber-Institute of the MPG *(for personal use only)* (www.fhi-berlin.mpg.de/ac)